Research Article

Bin Sun*, Huixian Zhang, and Yiming Wang

Research progress on Fe^{3+}-activated near-infrared phosphor

https://doi.org/10.1515/rams-2023-0160
received September 18, 2023; accepted December 07, 2023

Abstract: Fe^{3+}-activated near-infrared (NIR) luminescent materials have attracted widespread attention due to their tunable emission wavelength and extensive applications in various fields such as plant growth, food analysis, biomedical imaging, and night vision. Many excellent NIR materials have been developed by introducing non-toxic and environmentally friendly Fe^{3+} ions into different inorganic hosts. This article elucidates the luminescent properties of Fe^{3+} ions by combining the Tanabe–Sugano energy level diagram and the configuration coordinate model. The latest research progress on Fe^{3+}-doped NIR luminescent materials is outlined, summarizing the luminescent characteristics of various Fe^{3+}-doped materials, including emission wavelength, emission bandwidth, quantum efficiency, and thermal stability. Particularly, a detailed summary and analysis of the application areas of Fe^{3+}-doped NIR luminescent materials are provided. Finally, the future prospects and challenges faced by Fe^{3+}-doped NIR luminescent materials are presented. This review contributes to a deeper understanding of the luminescence mechanism of Fe^{3+} and the research progress of iron ion-doped luminescent materials, aiming to develop advanced Fe^{3+}-activated NIR luminescent materials with enhanced performance and explore new application fields.

Keywords: Fe^{3+}-doped, phosphors, NIR phosphors, food industry

*** Corresponding author: Bin Sun,** Key Laboratory of Resource Chemistry and Eco-environmental Protection in Tibetan Plateau of State Ethnic Affairs Commission, Key Laboratory of Nanomaterials and Nanotechnology of Qinghai Province, School of Chemistry and Chemical Engineering, Qinghai Minzu University, Xining, 810007, Qinghai, China, e-mail: 2023043@qhmu.edu.cn
Huixian Zhang, Yiming Wang: Key Laboratory of Resource Chemistry and Eco-environmental Protection in Tibetan Plateau of State Ethnic Affairs Commission, Key Laboratory of Nanomaterials and Nanotechnology of Qinghai Province, School of Chemistry and Chemical Engineering, Qinghai Minzu University, Xining, 810007, Qinghai, China

1 Introduction

Near-infrared (NIR) phosphors in the NIR range have been extensively studied due to their unique properties [1–8]. With the advancement of technology, researchers have developed numerous emerging applications utilizing NIR, which has made people's lives smarter, more convenient, and healthier [9–12]. Numerous fields benefit from the diverse applications of NIR phosphors in various industries. In the food industry, these powders play a crucial role in food inspection and quality control. They can be used to detect contaminants, monitor food freshness, and ensure compliance with safety standards. In biomedical imaging, NIR phosphors enable advanced imaging techniques, such as fluorescence microscopy and molecular imaging, allowing for enhanced visualization of tissues, cells, and biomolecules. Their use in drug delivery systems further contributes to targeted and controlled release of therapeutic agents. Beyond the realm of healthcare, NIR phosphors have proven invaluable in other industries as well. In agriculture, they facilitate plant growth monitoring by providing essential information about photosynthesis, nutrient uptake, and stress levels. In security and surveillance, these powders find application in night vision technology, enabling enhanced visibility in low-light conditions. Additionally, their unique properties are utilized in iris recognition systems, enhancing the accuracy and security of biometric identification. Furthermore, NIR phosphors have a significant impact on remote sensing technologies. They are employed in satellite imaging, allowing for the remote monitoring of environmental phenomena, weather patterns, and land use. This information aids in various fields, such as urban planning, natural resource management, and climate change studies. Figure 1 illustrates the diverse range of applications where NIR phosphors are employed, showcasing their versatility and contribution to multiple industries [13–15]. As research and development continue in this field, we can anticipate further advancements and the emergence of new applications, revolutionizing various sectors and improving our quality of life [16–24]. Trivalent rare earth ions such as Pr^{3+}, Nd^{3+}, Ho^{3+},

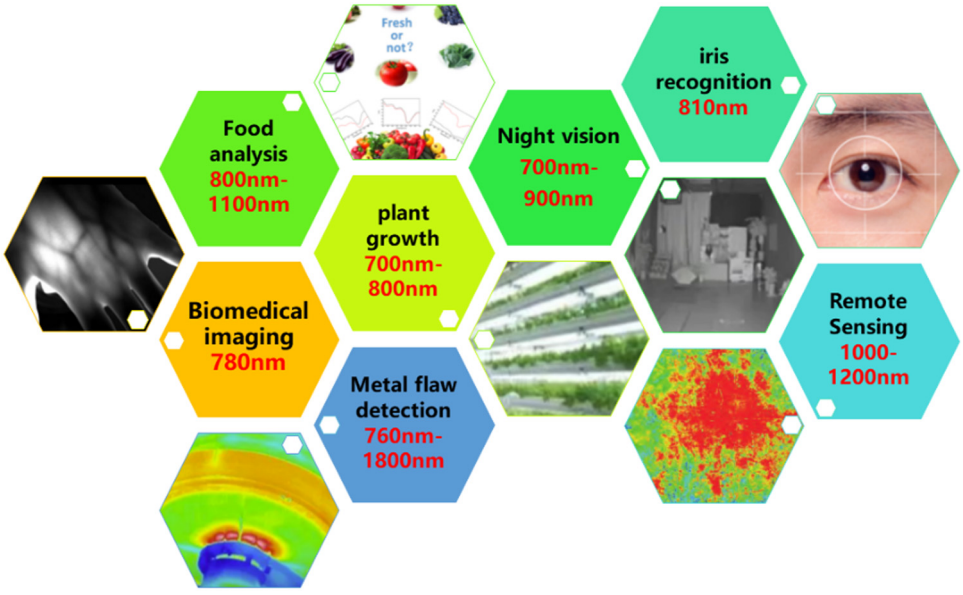

Figure 1: Target applications of NIR pc-LED with different emission wavelengths (730–1,800 nm) [39–46].

Er^{3+}, Tm^{3+}, and Yb^{3+} are capable of NIR emission [25–32]. However, the NIR emission produced by these trivalent rare earth ions is linear, which limits their applications in food inspection, night vision illumination, NIR spectroscopy, and other technologies. Eu^{2+} can generate broad band emission, but the emission peak is too close to the red region and does not meet the requirements [33–36]. The potential risk of Cr^{3+} oxidation to Cr^{6+} increases the toxicity of phosphors, limiting their long-term applications in the body. In recent years, Fe^{3+}-doped NIR phosphors for LED conversion have become one of the most promising NIR light sources, attracting widespread attention [37]. As an activator, Fe^{3+} has sparked wide interest among researchers. The rapid development of Fe^{3+}-doped NIR phosphors has greatly contributed to the advancement of broadband NIR phosphor-converted LEDs and their successful applications in medical and food detection, generating significant interest among scientists [38]. However, there are still some challenges in the application of Fe^{3+}-doped NIR phosphors, such as the need to improve the shorter emission wavelength and thermal stability. Further research is needed to develop wide-band and high-efficiency phosphors. This article provides an overview of the latest achievements in the study of Fe^{3+}-activated NIR phosphor. We summarize the research progress on the optical properties, structural characteristics, and luminescent mechanisms of Fe^{3+}-activated NIR phosphor [39–46].

2 Chemical synthesis

The crystal structure of the host lattice determines the coordination environment of the dopant ions, such as positional symmetry and interionic spacing. In this article, we provide a detailed description of the synthesis methods and experimental design used in the study. We discuss the selection of raw materials, reaction conditions, and preparation steps, and provide precise data and characterization methods for the experimental results. In terms of synthesis methods, researchers have developed various techniques for preparing Fe^{3+}-doped NIR phosphors. Sol–gel method, co-precipitation method, and thermal decomposition method, among others, have been widely used to prepare materials with excellent properties. In addition to conventional solid-state reaction methods, some novel synthesis strategies, such as hydrothermal method and microwave-assisted method, have also been adopted to achieve controlled morphology and structure.

3 Discussion

Phosphors doped with Fe^{3+} exhibit excellent NIR emission performance. These materials demonstrate tunable NIR luminescent properties within the range of 700–1,100 nm, closely related to their band structures, emissive centers, and interactions with activating ions. By controlling synthesis conditions, modifying the matrix, and adjusting the doping concentration, the emission intensity and peak of fluorescent materials can be customized to achieve the desired optical performance. We have discussed the series of fluorescent powders doped with Fe^{3+} from the following three perspectives: 1) Why choose Fe^{3+} as the activator and

the luminescent properties of Fe^{3+} ions; 2) Typical luminescent properties and research progress of Fe^{3+}-activated NIR phosphor; 3) Some application areas and potential of Fe^{3+}-activated NIR phosphor.

3.1 Why choose Fe^{3+} as the activator and the luminescent properties of Fe^{3+} ions?

Fe^{3+} is a non-rare earth element and one of the most abundant elements on Earth. The cost-effective extraction of Fe^{3+} from iron, along with its stable supply and wide availability of iron resources compared to other rare earth elements, makes Fe^{3+} more sustainable and reduces dependence on rare elements, thus saving energy. One of the important advantages of Fe^{3+} is its non-toxicity, which is crucial in many applications. The use of safe and non-toxic substances is particularly important in various fields, especially in medicine and biosciences, where Fe^{3+} dopants fulfill this requirement and are widely used in applications such as biomedical imaging, drug delivery, and biosensing. Additionally, Fe^{3+} possesses a unique energy level structure and tends to exhibit NIR emission in octahedral environments (which will be discussed in detail in the next section). These advantages make Fe^{3+} an ideal dopant for NIR applications.

As a typical ion with a $3d^5$ electron configuration, Fe^{3+} ion has five electrons in its outermost shell, with an electron configuration of $1s^2 2s^2 2p^6 3s^2 3p^6 3d^5$. The 3d electrons, being in the outermost shell, are significantly influenced by the surrounding crystal field. Therefore, the choice of matrix directly affects the luminescent properties of Fe^{3+} ions. It is known that Fe^{3+} ions can achieve NIR emission in an octahedral coordination environment. The energy level splitting of Fe^{3+} ions in an octahedral coordination environment is shown in the Tanabe–Sugano (T–S) diagram (Figure 2): the ground state term of this configuration is $^6A_1$ (^6S), the free electron term ^4G splits into $^4T_1$ and $^4T_2$, and the degenerate $^4A_1/^4E$ and ^4D splits into ^4E and $^4T_2$. The $^6A_1$ (^6S) term is a horizontal line, and the $^4A_1/^4E$ and ^4E terms are also horizontal, so their energy is independent of the crystal field. The transitions from the ground state to these three states should produce sharp peaks, while transitions to stronger ligand fields such as $^4T_1$ and $^4T_2$ will result in broader bands. Similar to the $3d^3$ electron configuration of Cr^{3+} ion, it can be observed from the T–S energy level diagram in Figure 2 that the emission wavelength of Fe^{3+} is strongly influenced by the crystal field strength. The values of octahedral crystal field parameters D_q, Racah parameters B and C, as well as the crystal field strength D_q/B, for Fe^{3+}-doped fluorescent powders can be estimated using the following equation [47]:

$$E(^6A_1(^6S) \rightarrow {}^4T_2(^4D)) = 13B + 5C, \quad (1)$$

$$E(^6A_1(^6S) \rightarrow {}^4E_2(^4D)) = 17B + 5C, \quad (2)$$

$$E(^6A_1(^6S) \rightarrow {}^4T_1(^4P)) = 18B + 7C, \quad (3)$$

$$E(^6A_1(^6S) \rightarrow {}^4T_1(^4G)) = 10D_q + 10B + 6C - (26B^2/10D_q), \quad (4)$$

$$E(^6A_1(^6S) \rightarrow {}^4T_2(^4G)) = 10D_q + 10B + 6C - (26B^2/10D_q). \quad (5)$$

Generally, the excitation of Fe^{3+}-doped NIR fluorescent powders originates from $^6A_1(^6S) \rightarrow {}^4E(^4D)$, $^6A_1(^6S) \rightarrow {}^4T_2(^4D)$

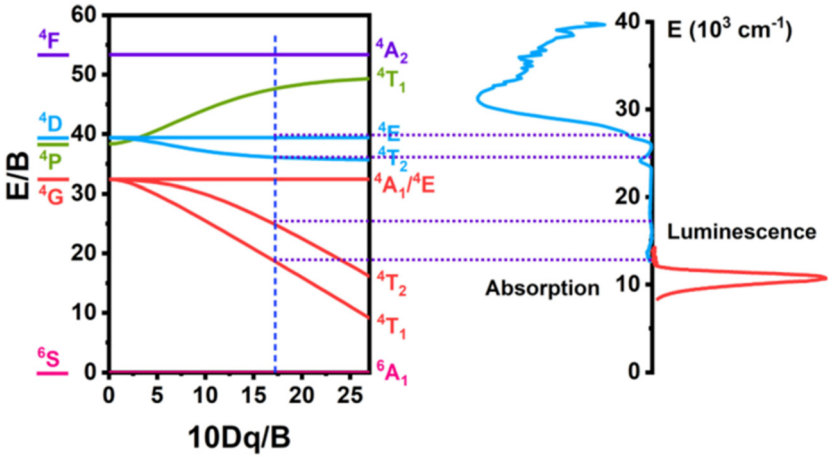

Figure 2: T–S energy-level diagram of the $3d^5$ electronic configuration in the octahedral field as well as the PLE and PL spectra of Fe^{3+} doping NIR phosphor [47].

and $^6A_1(^6S) \rightarrow {}^4T_2(^4G)$ transitions; the emission is due to the Fe^{3+} $^4T_1(^4G) \rightarrow {}^6A_1(^6S)$ of electronic transition. From the T–S diagram (Figure 2), it can be observed that the weaker the crystal field strength, the smaller the peak wavelength of the emitted light [47].

The d–d transitions of Fe^{3+} in octahedral sites are subject to the strict restriction of the Laporte selection rule. This limitation presents a challenge in achieving high luminescence efficiency for long-wavelength NIR emission in Fe^{3+}. The Laporte selection rule is a principle used to predict the spectroscopic activity of transition metal ions. According to this rule, charge transfer transitions are forbidden when the initial and final orbitals have the same symmetry. In the case of octahedral coordination, this means that d-electrons at the center of the octahedron cannot undergo transitions between the same spin orbitals, thus limiting the spectroscopic properties of octahedral complexes. Therefore, to achieve high luminescence efficiency for long-wavelength NIR emission in Fe^{3+}, it is necessary to modify the structure of octahedral complexes by altering the ligand environment or introducing additional modifications. This may involve selecting appropriate ligands, tuning the crystal field strength, or introducing external alkaline earth metals, among other approaches. While this task presents challenges, it also offers numerous opportunities and prospects for applications. Achieving high luminescence efficiency for long-wavelength NIR emission in Fe^{3+} will contribute to the development of efficient NIR emissive materials, which are of significant importance in fields such as optoelectronics, biomedical imaging, and energy conversion. Consequently, researchers have been exploring various methods to overcome the limitations imposed by the Laporte selection rule in order to achieve high luminescence efficiency for long-wavelength NIR emission in Fe^{3+}. The outcomes of these efforts will provide us with more choices of NIR emissive materials and drive further advancements and innovations in related fields.

3.2 Typical luminescent properties and research progress of Fe^{3+}-activated NIR phosphor

Recently reported Fe^{3+}-doped phosphors have emission wavelengths exceeding 800 nm. They have great potential for various applications, such as $CaAl_{12}O_{19}:Fe^{3+}$ (808 nm) [48], $SrAl_{12}O_{19}:Fe^{3+}$ (811 nm) [48], and $CaGa_2O_4:Fe^{3+}$ (809 nm) [49]. It offers a flexible design for new Fe^{3+}-doped NIR persistent phosphors through cation substitution and local crystal field modification. Table 1 summarizes some NIR phosphors doped with Fe^{3+}. In 2022, Wang reported unprecedented long-wavelength NIR emission phosphors of Fe^{3+}-activated $Sr_{2-y}Ca_y(InSb)_{1-z}Sn_{2z}O_6$ [50]. Overall emission tuning from 885 to 1,005 nm and full-width at half-maximum (FWHM) broadening from 108 to 146 nm were achieved through crystallographic site engineering strategies. NIR emission was significantly enhanced after complete Ca^{2+} incorporation due to the reduced symmetry induced by substitution. $Ca_2InSbO_6:Fe^{3+}$ phosphor exhibited a peak at 935 nm with an ultra-high internal quantum efficiencies (IQE) of 87%. The synthesized tunable emission phosphors showed enormous potential for NIR spectral detection. This work initiated the development of efficient Fe^{3+}-activated broadband NIR emission phosphors and opened up a new pathway for the design of NIR emitting phosphor materials. In 2022, Zhang *et al.* successfully synthesized Fe^{3+}-activated $NaScSi_2O_6$ phosphor [51]. Upon excitation at 300 nm UV light, a wide NIR emission band at 900 nm with an FWHM of 135 nm and an IQE of 13.3% was observed. The luminescence was related to the 3d–3d transitions of Fe^{3+} in octahedral coordination, confirming the effectiveness of Fe^{3+} activators in achieving efficient NIR emission. In 2022, Xiang *et al.* reported a series of environmentally friendly and low-cost Fe^{3+}-activated $ZnGa_2O_4$ phosphors [52]. The Fe^{3+}-doped phosphors exhibited a broad emission range from 650 to 850 nm, with a maximum emission peak at 720 nm and an

Table 1: Luminescence properties and related parameters of partial Fe^{3+}-activated NIR phosphor

Phosphor	PLE, PL (nm)	FWHM (nm)	IQE	*I*(%)@Temp.	Refs
$Sr_2InSbO_6:Fe^{3+}$	340, 885	108	48%	/	[55]
$Ca_2InSbO_6:Fe^{3+}$	340, 935	146	87%	/	[55]
$NaScSi_2O_6:Fe^{3+}$	300, 900	135	13.3%	/	[51]
$ZnGa_2O_4:Fe^{3+}$	344, 720	70	/	71%@423 K	[56]
$Mg_2SnO_4:Fe^{3+}$	308, 789	140	/	/	[57]
$NaAl_5O_8:Fe^{3+}$	346, 754	/	/	83.1%423 K	[54]
$Li_2ZnSiO_4:Fe^{3+}$	300, 750	/	62.7%	35.43%@373 K	[58]
$Li_2ZnGeO_4:Fe^{3+}$	300, 777	/	30.57%	49.79%@373 K	[58]
$Sr_9Ga(PO_4)_7:Fe^{3+}$	330, 915	155	6.6%	50%@260 K	[47]

FWHM of 70 nm. The emission intensity remained at 71% even at an elevated temperature of 423 K. The NIR pc-LED made of this phosphor exhibited strong NIR emission. In 2023, Li *et al.* reported a novel Fe^{3+}-activated NIR persistent phosphor composed of Mg_2SnO_4 [53]. Fe^{3+} ions occupied both tetrahedral and octahedral sites, and due to the energy level alignment, electrons released from traps preferentially returned to the excited energy level of Fe^{3+} in the tetrahedral sites *via* tunneling, resulting in efficient NIR persistent emission at a peak wavelength of 789 nm with an FWHM of 140 nm. This phosphor demonstrated a record-breaking persistence duration of over 31 h in Fe^{3+}-based phosphors for night vision applications, serving as a self-sustainable light source. This work not only provided a new type of efficient Fe^{3+}-doped NIR persistent phosphor for technological applications but also established practical guidelines for the rational tuning of persistent emission. Based on the analysis and summary of the above literature, it can be observed that a disadvantage of Fe^{3+}-doped NIR phosphors is the inability to be efficiently excited by blue light, which limits their applications to some extent. In 2023, Cheng *et al.* synthesized Fe^{3+}-activated $NaAl_5O_8$ NIR phosphors [54]. Under excitation at 346 nm, $NaAl_5O_8$:Fe^{3+} phosphors exhibited NIR emission with a main peak at 754 nm. Emission spectra were measured in the temperature range of 303–463 K, revealing that the emission intensity at 423 K remained at 83.1% of that at 303 K, indicating excellent thermal stability of the sample. The luminescent behavior of the sample was studied after immersing it in deionized water for 0–10 h. These findings suggest that $NaAl_5O_8$:Fe^{3+} samples hold promise for applications in high-temperature or humid environments. Furthermore, the use of $NaAl_5O_8$:Fe^{3+} in the preparation of anti-counterfeit ink demonstrated its potential in the field of anti-counterfeiting. In 2023, Yang *et al.* synthesized Fe^{3+}-activated Li_2ZnAO_4 (A = Si, Ge) phosphors through solid-state reactions, with Fe^{3+} occupying the tetrahedral sites of Zn^{2+} [38]. Under excitation by 300 nm ultraviolet light, broad NIR emission bands were observed at 750 nm (Li_2ZnSiO_4:Fe^{3+}) and 777 nm (Li_2ZnGeO_4:Fe^{3+}), with IQE of 62.70% (Li_2ZnSiO_4:Fe^{3+}) and 30.57% (Li_2ZnGeO_4:Fe^{3+}). The thermal stability at 373 K was improved from 35.43 to 49.79% through cation tuning. The combination of activation energy, electron-phonon coupling, and Debye temperature explained the enhanced thermal stability of Li_2ZnGeO_4:Fe^{3+} phosphors. Additionally, the synthesized phosphors exhibited sensitive and selective detection of Cu^{2+} ions. In 2023, the research team led by Quanlin Liu utilized the structural confinement effect in $Sr_9Ga(PO_4)_7$ (SGP) to selectively control energy transfer pathways, suppressing luminescence concentration and thermal quenching effects. They found that in Fe^{3+}-doped SGP compounds, the relatively large Fe^{3+}-Fe^{3+} distances hindered energy transfer between Fe^{3+} ions, resulting in weakened concentration quenching. The $Sr_9Ga_{0.8}(PO_4)_7$:0.2Fe^{3+} (SGP:0.2Fe^{3+}) phosphor exhibited the highest NIR luminescence intensity. Additionally, they introduced trivalent Yb^{3+} to investigate its influence on the luminescence of Fe^{3+}-doped phosphor systems. Co-doping Yb^{3+} into SGP:0.2Fe^{3+} resulted in much shorter Fe^{3+}–Yb^{3+} distances compared to Fe^{3+}–Fe^{3+}, facilitating rapid energy transfer from the quenching center Fe^{3+} to the thermally stable center Yb^{3+}. The thermal stability of SGP:0.2Fe^{3+} ,0.07Yb^{3+} was greatly enhanced compared to SGP:0.2Fe^{3+}. This study provided a method to enhance NIR luminescence by utilizing structural confinement to control energy transfer pathways and suppress concentration and thermal quenching effects. Finally, they demonstrated the potential applications of SGP:0.2Fe^{3+} and SGP:0.2Fe^{3+} ,0.07Yb^{3+} phosphors in the fields of night vision and optical thermometry [47].

3.3 Some application areas and potential of Fe^{3+}-activated NIR phosphor

The phosphor activated by Fe^{3+} ions distinguishes itself through its superior optical properties, which significantly amplify its application potential across diverse fields. These properties, encompassing high luminescence efficiency and exceptional stability, pave the way for its use in advanced imaging, plant growth, food analysis, biomedical imaging, and night vision. Next, let's take the application in the field of anti-counterfeiting as an example to demonstrate. In 2023, Cheng *et al.* presented their findings on Fe^{3+}-activated $NaAl_5O_8$ NIR phosphor, examining its phase and luminescent properties [54]. It was observed that the optical bandgap narrows as the Fe^{3+} doping concentration increases. The sample's thermal stability was confirmed by maintaining 83.1% emission intensity at 423 K compared to 303 K, as measured across an emission spectrum range of 303–463 K. These research results not only demonstrate the potential applications of $NaAl_5O_8$:Fe^{3+} samples in high temperature or humid environments but also highlight their significance in the field of anti-counterfeiting, particularly in the context of anti-counterfeiting inks. Anti-counterfeiting inks are widely used in the protection of important documents such as currency, identification cards, and labels to prevent forgery and fraud. By utilizing $NaAl_5O_8$:Fe^{3+} as a phosphor material in anti-counterfeiting inks, enhanced anti-counterfeiting effects can be achieved. There are several advantages of incorporating $NaAl_5O_8$:Fe^{3+} in anti-counterfeiting inks. First, $NaAl_5O_8$:Fe^{3+} phosphor exhibits high stability and

is resistant to high temperatures, allowing it to maintain its luminescent properties in environments with elevated temperatures. This is crucial during the manufacturing process of anti-counterfeiting inks, which often involves heating and curing. Second, $NaAl_5O_8:Fe^{3+}$ phosphor demonstrates good stability in humid environments, preventing performance degradation associated with humidity and ensuring the ink's reliability and durability in such conditions. Furthermore, the successful application of $NaAl_5O_8:Fe^{3+}$ in anti-counterfeiting has been verified. Figure 3 illustrates the remarkable efficacy of $NaAl_5O_8:Fe^{3+}$ when utilized as an anti-counterfeiting ink. The phosphor's luminescent qualities are uniquely tailored, exhibiting distinct spectral features that can be precisely identified and authenticated. These tailored characteristics render the ink exceptionally conspicuous and swiftly verifiable, ensuring its integrity is effortlessly ascertainable with the employment of specialized detection apparatus or analytical instruments. This not only underscores the ink's suitability for high-security applications but also enhances its practicality for widespread use in safeguarding valuable items from counterfeiting attempts. Hence, the successful utilization of $NaAl_5O_8:Fe^{3+}$ phosphor as a constituent in anti-counterfeiting inks not only underscores its significance in the realm of anti-counterfeiting but also serves as a pivotal tool in the ongoing battle against counterfeit currency and forged identification cards. Furthermore, its implementation plays a crucial role in safeguarding brand integrity, fortifying fraud deterrents, and upholding consumer trust. These groundbreaking research findings provide compelling evidence to propel the advancement of anti-counterfeiting technologies, paving the way for new avenues of innovation and progress in combating counterfeit practices [54].

Moreover, apart from its applications in anti-counterfeiting technology, NIR phosphors doped with Fe^{3+} have also demonstrated remarkable potential in the field of night vision. In 2023, Li *et al.* reported that Fe^{3+}-doped NIR phosphor demonstrated a record-breaking duration of over 31 h, making it a self-sustainable light source for night vision applications, as shown in Figure 4 [57].

Phosphors doped with Fe^{3+} ions have broad prospects in applications such as luminescence thermometry and NIR stickers. In 2022, Zhang *et al.* conducted a study on Fe^{3+}-activated $NaScSi_2O_6$ phosphor [51]. In their research, they excited the sample with 300 nm ultraviolet light and observed a broad NIR emission band at 900 nm, with an FWHM of 135 nm and an IQE of 13.3%. This emission behavior is closely related to the 3d–3d transitions of Fe^{3+} ions in octahedral sites, validating the effectiveness of Fe^{3+} as an activator for achieving efficient NIR emission. The research results also showed that the emission intensity of Fe^{3+} exhibited a linear quenching trend within the temperature range of 293–433 K. This indicates that Fe^{3+}-doped phosphor can serve as a sensitive luminescent temperature sensing material, and the changes in its emission intensity can be used for real-time temperature measurement and monitoring. In addition, the feasibility of the synthesized phosphor material was also investigated in applications such as NIR luminescence thermometry and NIR stickers, as shown in Figure 5. This implies that Fe^{3+}-doped phosphor has potential applications in non-contact temperature measurement technologies and patch-type infrared sensors. These applications contribute to achieving high-precision, high-sensitivity, and long-distance temperature measurements, providing more possibilities for industries such as industrial production, energy utilization, and medical diagnostics. In summary, Fe^{3+}-doped phosphor exhibits tremendous potential in applications such as luminescence thermometry and NIR stickers. The compelling research findings surrounding Fe^{3+}-doped phosphor offer robust

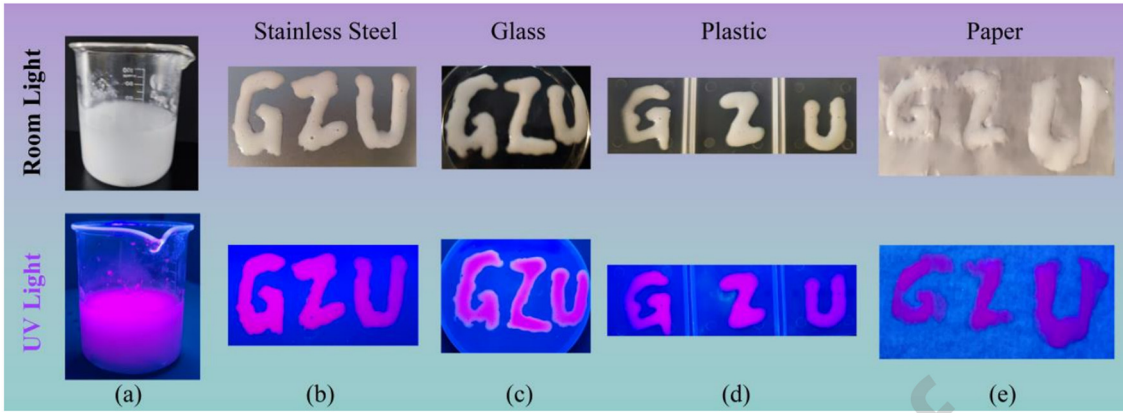

Figure 3: Security inks (a) and the patterns written on (b) stainless steel, (c) glass, (d) plastic, and (e) paper under room light and UV light [54].

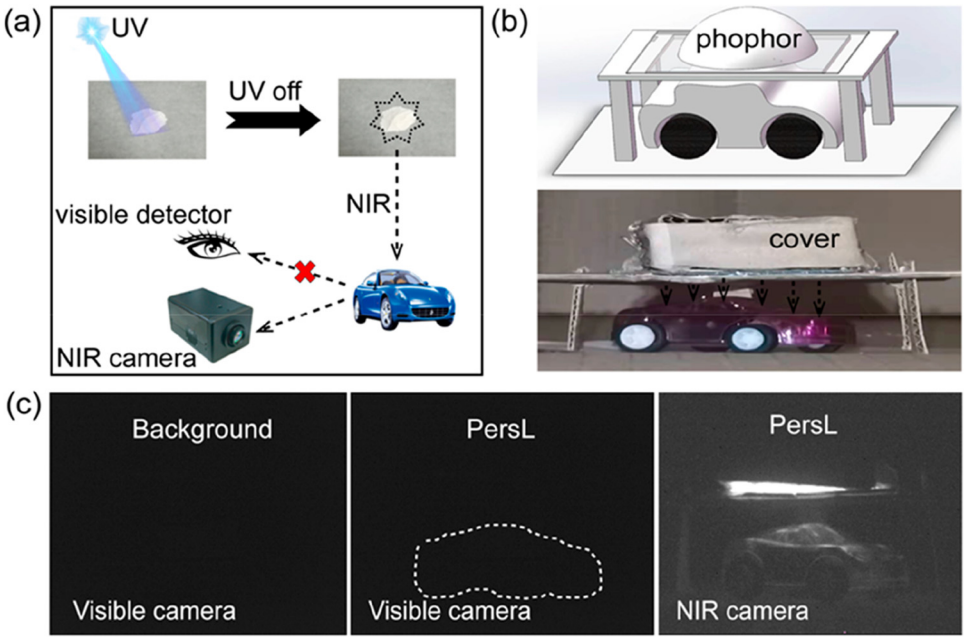

Figure 4: Schematic (a) and experimental setup (b) for the self-sustainable night vision imaging. (c) Photos of a toy car taken in the dark with and without NIR PersL illumination by visible and NIR cameras [57].

evidence, bolstering the case for its continued development and expanded utilization within the realm of infrared luminescence. The intrinsic properties of this material, such as its efficient infrared emission and stable luminescent behavior under varying conditions, lay a solid foundation for breakthroughs in technological innovation. Moreover, these findings illuminate a path forward for application development in fields including, but not limited to, bioimaging, security, and optical communications. The promising results obtained thus far herald a new era of advancements, underscoring the transformative potential of Fe^{3+}-doped phosphor in driving forward the frontiers of infrared luminescent applications [51].

Research has found that the majority of Fe^{3+}-doped NIR fluorescent materials exhibit lower IQE values. It is noteworthy that Fe^{3+}-doped NIR fluorescent materials have broad absorption bands. This broad band feature allows them to absorb more light energy, thereby enhancing the efficiency of light excitation. This is crucial for

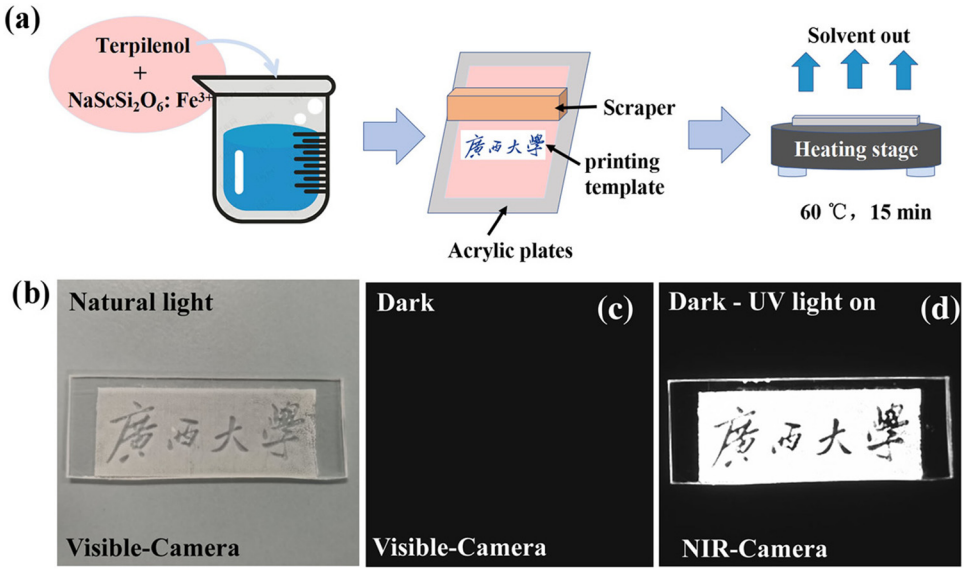

Figure 5: (a) Scheme of the fabrication of an IR patch by the screen printing method. Photographs under natural light captured using a visible camera (b, left) and in the dark captured using a NIR camera under UV excitation light when it is off (c, middle) and on (d, right) [51].

applications such as bioimaging and photovoltaics, as it can provide stronger excitation signals or higher energy conversion efficiency. Additionally, Fe^{3+}-doped NIR fluorescent materials have relatively long lifetimes. The lifetime of fluorescent materials is critical for the stability and optical performance of fluorescent probes. A longer lifetime can reduce background noise in fluorescence bioimaging, improve imaging clarity and signal-to-noise ratio, and also benefit the stability and long-term use of photovoltaic devices.

Unfortunately, the understanding of the luminescence mechanism and certain related luminescent properties of Fe^{3+}-doped NIR phosphors is not yet sufficiently deep. Although some studies have revealed key luminescence mechanisms and band structures, further research is still needed to address some of the complexities involved. Second, the stability of Fe^{3+}-doped NIR fluorescent materials needs to be improved. Some studies indicate that certain fluorescent materials undergo degradation or irreversible deactivation of fluorescence intensity under prolonged excitation or high-temperature environments. This instability limits the further promotion and application scope of the materials in practical use. Additionally, the selection of matrix materials and optimization of structural design remain challenging. The choice of matrix and novel structural design significantly impact the improvement of optical performance. It is necessary to consider the balance of ion concentration with fluorescence efficiency, lifetime, and light absorption intensity to obtain better optical performance.

In conclusion, Fe^{3+}-doped NIR fluorescent materials have a wide range of optical performance advantages, including broad emission wavelength range, high fluorescence quantum yield, wide light absorption band, and relatively long lifetime. However, challenges regarding understanding the mechanism, stability, and structural design still need to be addressed. Future research will focus on overcoming these challenges and further improving and optimizing the optical performance of Fe^{3+}-doped NIR fluorescent materials to achieve their widespread application in fields such as biomedical imaging and optoelectronics.

4 Outlook and challenges

4.1 Outlook

Looking ahead, with the increasing demand for NIR fluorescent materials, Fe^{3+}-doped NIR fluorescent materials are expected to find more applications in a wider range of fields. In the field of biomedical imaging, Fe^{3+}-doped NIR fluorescent materials have great potential in tumor labeling, early cancer detection, and photodynamic therapy due to the deep penetration ability of NIR light and low tissue autofluorescence interference. In the field of biosensors, Fe^{3+}-doped NIR fluorescent materials have high sensitivity and selectivity, enabling efficient, rapid, and accurate detection of biomolecules, providing strong support for disease diagnosis and drug screening. Additionally, Fe^{3+}-doped NIR fluorescent materials have a wide range of application prospects in the field of photovoltaics, which can improve photovoltaic conversion efficiency and energy output, providing new possibilities for the development and utilization of renewable energy. In summary, significant progress has been made in the research of Fe^{3+}-doped NIR phosphors due to their tunable luminescent properties and potential applications in the NIR spectral range, making them a hot research topic. Further research will help to understand its luminescence mechanism, improve its luminescence efficiency and stability, and expand its application prospects in the fields of biomedical imaging and optoelectronics.

4.2 Challenges

Although in recent years, Fe^{3+}-doped NIR fluorescent materials have been widely studied and received extensive attention due to their unique optical properties and potential applications, significant progress has already been made in the fields of biomedical imaging, biosensors, and photovoltaics. However, there are still challenges that need to be addressed in current research. For example, some Fe^{3+}-doped NIR phosphors still exhibit issues with long-term excitation and stability, which limits their further advancement in practical applications. Additionally, further research is needed to deepen our understanding of the Fe^{3+} doping mechanism and luminescent properties.

First, in the realm of preparation and synthesis, it is crucial to embark on further exploration and refinement of suitable synthesis methods and process conditions. As the current preparation methods possess certain complexities and challenges in controlling material parameters, it is imperative to undertake more research to discover efficient, controllable, and reproducible preparation techniques. Additionally, to bolster the efficiency and stability of fluorescence, a more comprehensive understanding of the Fe^{3+} doping mechanism and luminescent properties becomes indispensable in facilitating enhanced material design and synthesis.

Second, emphasis should be placed on material stability and long-term reliability. The challenges lie in mitigating light attenuation and degradation, which can adversely

impact luminescence performance in prolonged excitation and high-temperature environments. To tackle this predicament, it is imperative to develop more robust materials, including enhancing the light damage threshold and augmenting their optical durability. These advancements will enhance stability and render them more suitable for practical applications.

Additionally, to further enhance luminescent performance, structural design improvements, crystal structure enhancement, and doping methods can be implemented. In particular, optimizing the doping concentration and dopants is an important research direction with the potential to achieve optimal control of material properties and luminescence efficiency. Furthermore, exploring novel synthesis techniques and the influence of external factors, such as temperature and pressure, on luminescent properties may offer additional avenues for improving material performance.

In summary, Fe^{3+}-doped NIR fluorescent materials hold immense promise and potential for applications in biomedical imaging, biosensors, and photovoltaics. Nevertheless, certain challenges persist in terms of preparation methods, stability, and luminescent performance. Future research efforts will be directed toward overcoming these challenges, enhancing the performance and stability of Fe^{3+}-doped NIR fluorescent materials, expanding their application prospects, and expediting their translation and utilization in the fields of biomedical imaging and optoelectronics.

Acknowledgments: This work was supported by the "Kunlun Talents - High-level Innovation and Entrepreneurial Talents" project (Elite Talents Project) in Qinghai Province. The work was finished with the help of Huixian Zhang and Yiming Wang.

Funding information: This work was supported by the "Kunlun Talents - High-level Innovation and Entrepreneurial Talents" project (Elite Talents Project) in Qinghai Province.

Author contributions: All authors have accepted responsibility for the entire content of this manuscript and approved its submission.

Conflict of interest: The authors state no conflict of interest.

References

[1] Miao, S., Y. Liang, Y. Zhang, D. Chen, and X. J. Wang. Blue LED-pumped broadband short-wave infrared emitter based on $LiMgPO_4:Cr^{3+}$, Ni^{2+} phosphor. *Advanced Materials Technologies*, Vol. 7, No. 11, 2022, pp. 2200320–2200329.

[2] Bai, B., P. Dang, Z. Zhu, H. Lian, and J. Lin. Broadband near-infrared emission of $La_3Ga_5GeO_{14}:Tb^{3+}$, Cr^{3+} phosphors: energy transfer, persistent luminescence and application in NIR light-emitting diodes. *Journal of Materials Chemistry C*, Vol. 8, No. 34, 2020, pp. 11760–11770.

[3] Gao, T., W. Zhuang, R. Liu, Y. Liu, and Y. Xue. Design and control of the luminescence in Cr^{3+}-doped NIR phosphors via crystal field engineering. *Journal of Alloys and Compounds*, Vol. 848, No. 246, 2020, pp. 156557–156565.

[4] Xixi, Q., W. Dakun, Q. Jianrong, Y. Qin, M. Zhijun, and L. Shijian. Inducing NIR long persistent phosphorescence in Cr-doped perovskite titanate via redox. *Journal of Alloys and Compounds*, Vol. 666, No. 2, 2016, pp. 387–391.

[5] Yang, S., Y. Wang, G. Xiang, S. Jiang, L. Li, F. Ling, et al. Luminescence properties and phase transformation of broadband NIR emitting $A_2(WO_4)_3:Cr^{3+}$ (A=Al^{3+}, Sc^{3+}) phosphors toward NIR spectroscopy applications. *Journal of Luminescence*, Vol. 253, 2023, pp. 119445–119454.

[6] Xiang, J., J. Zheng, X. Zhao, X. Zhou, C. Chen, M. Jin, et al. Synthesis of broadband NIR garnet phosphor $Ca_4ZrGe_3O_{12}$: Cr^{3+}, Yb^{3+} for NIR pc-LED applications. *Materials Chemistry Frontiers*, Vol. 6, No. 4, 2022, pp. 440–449.

[7] Wu, H., L. Jiang, K. Li, C. Li, and H. Zhang. Design of broadband near-infrared $Y_{0.57}La_{0.72}Sc_{2.71}(BO_3)_4:Cr^{3+}$ phosphors based on one-site occupation and their application in NIR light-emitting diodes. *Journal of Materials Chemistry C*, Vol. 9, No. 35, 2021, pp. 11761–11771.

[8] Song, Q., Z. Liu, H. Jiang, Z. Luo, P. Sun, G. Liu, et al. The hydrothermally synthesis of $K_3AlF_6:Cr^{3+}$ NIR phosphor and its performance optimization based on phase control. *Journal of the American Ceramic Society*, Vol. 104, No. 10, 2021, pp. 5235–5243.

[9] Jakka, S. K., M. J. Soares, M. P. F. Grata, A. J. Neves, P. C. Nagajyothi, and K. Pavani. Thermal sensing in NIR to visible upconversion of Ho^{3+} and Yb^{3+} doped yttrium oxyfluoride phosphor. *Optical Materials*, Vol. 129, 2022, pp. 112442–112450.

[10] Mao, M., T. Zhou, H. Zeng, L. Wang, and R. J. Xie. Broadband near-infrared (NIR) emission realized by the crystal-field engineering of $Y_{3-x}Ca_xAl_{5-x}Si_xO_{12}:Cr^{3+}$ (x = 0–2.0) garnet phosphors. *Journal of Materials Chemistry C*, Vol. 8, No. 6, 2020, pp. 1981–1988.

[11] Yuan, S., Z. Mu, L. Lou, S. Zhao, D. Zhu, and F. Wu. Broadband NIR-II phosphors with Cr^{4+} single activated centers based on special crystal structure for nondestructive analysis. *Ceramics International*, Vol. 48, No. 18, 2022, pp. 26884–26893.

[12] Liu, S., H. Cai, S. Zhang, Z. Song, Z. Xia, and Q. Liu. Site engineering strategy toward enhanced luminescence thermostability of a Cr^{3+}-doped broadband NIR phosphor and its application. *Materials Chemistry Frontiers*, Vol. 5, No. 10, 2021, pp. 3841–3849.

[13] Chi, F., W. Dai, S. Liu, L. Qiu, X. Wei, Y. Chen, et al. Luminescence properties of Cr^{3+}-doped $Al_6Ge_2O_{13}$ broadband near-infrared phosphor. *Optical Materials*, Vol. 126, 2022, pp. 112218–112225.

[14] Zhou, Z., X. Yi, P. Xiong, X. Xu, Z. Ma, and M. Peng. Cr^{3+}-Free near-infrared persistent luminescence material $LiGaO_2$: Fe^{3+}: Optical properties, afterglow mechanism and potential bioimaging. *Journal of Materials Chemistry C*, Vol. 8, 2020, pp. 14100–14108.

[15] Pan, Z., Y. Y. Lu, and F. Liu. Sunlight-activated long-persistent luminescence in the near-infrared from Cr^{3+}-doped zinc gallogermanates. *Nature Materials*, Vol. 11, No. 1, 2012, pp. 58–63.

[16] Dai, D., Z. Wang, Z. Xing, X. Li, C. Liu, L. Zhang, et al. Broad band emission near-infrared material $Mg_3Ga_2GeO_8$: Cr^{3+}: Substitution of Ga-In, structural modification, luminescence property and

application for high efficiency LED. *Journal of Alloys and Compounds*, Vol. 806, 2019, pp. 926–938.

[17] Zhang, G., W. Wang, Y. Chen, X. Li, Y. Zhao, and L. Yang. Synthesis and luminescence properties of a novel deep red phosphor $Li_2ZnTi_3O_8:Mn^{4+}$ for plant-cultivation. *Spectrochimica acta, Part A. Molecular and Biomolecular Spectroscopy*, Vol. 240, No. 1, 2020, pp. 118567–118575.

[18] Zhang, S., Y. Liu, and J. Yin. A novel Cr^{3+}-activated far-red titanate phosphor: synthesis, luminescence enhancement and application prospect. *Materials Today Chemistry*, Vol. 24, No. 24, 2022, pp. 100835–100843.

[19] Shi, Y., Z. W. P. Envelope, J. Peng, Y. Wang, S. He, J. Li, et al. Achieving the ultra-broadband near-infrared $La_3SnGa_5O_{14}:Cr^{3+}$ phosphor via multiple lattice sites occupation for biological non-destructive detection and night-vision technology. *Materials Today Advances*, Vol. 16, pp. 100305–100313.

[20] Rogel-Castillo, C., R. B. Boulton, A. Opastpongkarn, G. Huang, and A. E. Mitchell. Use of near-infrared spectroscopy and chemometrics for the nondestructive identification of concealed damage in raw almonds (Prunus dulcis). *Journal of Agricultural & Food Chemistry*, Vol. 64, No. 29, 2016, pp. 5958–5962.

[21] Savita, V., P. Vashishtha, G. Gupta, A. Vij, and A. Thakur. UV/blue/green converted efficient red-NIR photoluminescence in Cr incorporated $MgAl_2O_4$ nanocrystals: Site selective emission tailored through cation inversion and intrinsic defects. *Journal of Physics: Condensed Matter*, Vol. 35, No. 11, 2023, pp. 115303–115311.

[22] Panda, S., P. Vinodkumar, M. Sahoo, U. Madhusoodanan, and B. S. Panigrahi. Probing the site occupancy of dopants in deep red-NIR emitting $LiAl_5O_8$: Eu^{3+}, Cr^{3+} and Fe^{3+} nano phosphors using photoluminescence and X-ray absorption spectroscopy - ScienceDirect. *Journal of Alloys and Compounds*, Vol. 857, 2020, pp. 157615–157623.

[23] Jüstel, T., V. Anselm, A. Meijerink, and B. Malysa. Energy Transfer From Cr^{3+} to Nd^{3+} in $GdAl_3(BO_3)_4$, $SrAl_{12}O_{19}$ and $SrGa_{12}O_{19}$. *Journal of Materials Research and Technology*, Vol. 11, 2016, pp. 785–791.

[24] Jiang, L., X. Jiang, J. Xie, T. Zheng, G. Lv, and Y. Su. Structural induced tunable NIR luminescence of $(Y,Lu)_3(Mg,Al)_2(Al,Si)_3O_{12}$: Cr^{3+} phosphors. *Journal of Luminescence*, Vol. 247, 2022, pp. 118911–118920.

[25] Giulio, G., C. Alessandro, P. Stefano, P. Laura, D. Alicia, and M. J. Pascual. Transparent oxyfluoride nano-glass ceramics doped with Pr^{3+} and Pr^{3+}–Yb^{3+} for NIR emission. *Frontiers in Materials*, Vol. 3, 2017, pp. 58–72.

[26] Nunes, L. R. R., H. P. Labaki, F. J. Caixeta, and R. R. Goncalves. Yb^{3+} influence on NIR emission from Pr^{3+}-doped spherical yttria nanoparticles for advances in NIR I and NIR II biological windows. *Journal of Luminescence*, Vol. 241, 2022, pp. 118485–118493.

[27] Baklanova, Y. V., O. A. Lipina, L. G. Maksimova, A. P. Tyutyunnik, I. I. Leonidov, T. A. Denisova, et al. Nd^{3+}, Ho^{3+}-codoped garnet-related $Li_7La_3Hf_2O_{12}$ phosphor with NIR luminescence. *Spectrochim Acta A Mol Biomol Spectrosc*, Vol. 180, 2017, pp. 105–109.

[28] Li, W., Q. He, J. Xu, C. Shao, S. Sun, S. Fan, et al. Efficient NIR to NIR up-conversion in $LiYF_4:Yb^{3+},Tm^{3+}$ micro-octahedrons by modified hydrothermal method. *Journal of Luminescence*, Vol. 227, 2020, pp. 117396–117400.

[29] İlhan, M., İ.Ç. Keskin, Z. Çatalgöl, and R. Samur. NIR photoluminescence and radioluminescence characteristics of Nd^{3+} doped $BaTa_2O_6$ phosphor. *International Journal of Applied Ceramic Technology*, Vol. 15, No. 6, 2018, pp. 1594–1601.

[30] Li, L., Y. Zhou, F. Qin, Y. Zheng, and Z. Zhang. On the Er^{3+} NIR photoluminescence at 800 nm. *Optics Express*, Vol. 28, No. 3, 2020, pp. 3995–3999.

[31] Xia, L., Y. Zhang, J. Ding, C. Li, X. Shen, and Y. Zhou. $Er^{3+}/Tm^{3+}/Nd^{3+}$ tri-doping tellurite glass with ultra-wide NIR emission. *Journal of Alloys and Compounds*, Vol. 863, No. 1, 2021, pp. 158626–158634.

[32] Unnikrishnan, V. N., C. Joseph, R. P. Biju, C. Jayakrishnan, and S. M. Sajna. NIR emission studies and dielectric properties of Er^{3+}-doped multicomponent tellurite glasses. *Spectrochimica Acta, Part A. Molecular and Biomolecular Spectroscopy*, Vol. 161, No. 12, 2016, pp. 130–137.

[33] Zhang, Q., X. Wang, Z. Tang, and Y. Wang. A $K_3ScSi_2O_7:Eu^{2+}$ based phosphor with broad-band NIR emission and robust thermal stability for NIR pc-LEDs. *Chemical Communications*, Vol. 56, No. 34, 2020, pp. 4644–4647.

[34] Yang, Z., Y. Zhao, Y. Zhou, J. Qiao, Y. C. Chuang, M. S. Molokeev, et al. Giant red-shifted emission in $(Sr,Ba)Y_2O_4:Eu^{2+}$ phosphor toward broadband near-infrared luminescence. *Advanced Functional Materials*, Vol. 32, No. 1, 2021, pp. 2103927–2103935.

[35] Tang, Z., F. Du, H. Liu, Z. Leng, X. Sun, H. Xie, et al. Eu^{2+}-Doped layered double borate phosphor with ultrawide near-infrared spectral distribution in response to ultraviolet–blue light excitation. *Advanced Optical Materials*, Vol. 10, No. 5, 2022, pp. 2102204–2102212.

[36] Zhu, Y., X. Wang, J. Qiao, M. S. Molokeev, H. C. Swart, L. Ning, et al. Regulating Eu^{2+} multisite occupation through structural disorder toward broadband near-infrared emission. *Chemistry of Materials*, Vol. 35, No. 3, pp. 1432–1439.

[37] Liu, G., S. Zhang, and Z. Xia. Multi-sites energy transfer in Fe^{3+}-doped $KAl_{11}O_{17}$ phosphor toward zero thermal quenching near-infrared luminescence. *Optics Letters*, Vol. 48, No. 5, 2023, pp. 1296–1304.

[38] Yang, Y., L. Shen, J. Zhang, S. Zhao, Q. Pang, X. Zhang, et al. Tetracoordinate Fe^{3+} Activated Li_2ZnAO_4 (A= Si, Ge) Near-Infrared Luminescent Phosphors. *Inorganic Chemistry*, Vol. 62, No. 32, 2023, pp. 12862–12871.

[39] Wei, G., P. Li, R. Li, Y. Wang, S. He, J. Li, et al. How to achieve excellent luminescence properties of Cr Ion-doped near-infrared phosphors. *Advanced Optical Materials*, Vol. 40, pp. 2301794–23017814.

[40] Song, L., S. Liang, W. Nie, X. He, J. Hu, F. Lin, et al. Ultra-broad near-infrared emitting phosphor $LiInF_4:Cr^{3+}$ with extremely weak crystal field. *Inorganic Chemistry*, Vol. 62, No. 28, 2023, pp. 11112–11120.

[41] Huang, W. T., K. C. Chen, M. H. Huang, and R. S. Liu. Tunable spinel structure phosphors: Dynamic change in near-infrared windows and their applications. *Advanced Optical Materials*, Vol. 40, 2023, pp. 2301166–2301188.

[42] Gao, F., W. U. Khan, Z. Cheng, W. U. Khan, I. Ahmad, Z. Ye, et al. Efficient ultra-broadband phosphors for high-power near-infrared LED and night vision imaging system sources. *Dyes and Pigments*, Vol. 219, 2023, pp. 111632–111642.

[43] Guo, G., Q. Xi, T. Yin, J. Nie, Y. Zhang, L. Guan, et al. Ultra-broadband near-infrared phosphor $La_2CaTa_xZr_{(1-x)}O_6$: Cr^{3+} for phosphor-converted light-emitting diodes. *Journal of Alloys and Compounds*, Vol. 965, 2023, pp. 171459–171467.

[44] Li, Z., G. Zhu, S. Li, W. Xu, Q. Bian, Y. Cong, et al. High-performance NIR emission in chromium-doped garnet phosphors enabled by structure and excitation regulation. *Laser & Photonics Reviews*, Vol. 20, pp. 2300732–2300754.

[45] Shao, Z., X. Zhou, L. Li, Y. Wang, F. Ling, C. Jing, et al. Broadband near-infrared double-perovskite phosphor Sr_2ScTaO_6: Cr^{3+}, Yb^{3+} for NIR pc-LED applications. *Ceramics International*, Vol. 49, No. 20, 2023, pp. 32860–32867.

[46] Wang, J., X. Wang, C. Zhang, X. Zhang, T. Zhou, and R.-J. Xie. Broadband emitting phosphor $Sr_6Sc_2Al_4O_{15}$:Cr^{3+} for near-infrared LEDs. *Journal of Materials Chemistry C*, Vol. 11, 2023, pp. 9030–9036.

[47] Zhao, F., Y. Shao, Z. Song, and Q. Liu. Structural confinement toward suppressing concentration and thermal quenching for improving near-infrared luminescence of Fe^{3+}. *Inorganic Chemistry Frontiers*, Vol. 10, 2023, pp. 6701–6710.

[48] Li, Y. J., Y. Y. Ma, S. Ye, G. P. Hu, and Q. Y. Zhang. Site-related near-infrared luminescence in $MAl_{12}O_{19}$ (M = Ca, Sr, Ba):Fe^{3+} phosphors. *Materials Research Bulletin*, Vol. 51, 2014, pp. 1–5.

[49] Kniec, K., W. Piotrowski, K. Ledwa, L. D. Carlos, and L. Marciniak. Spectral and thermometric properties altering through crystal field strength modification and host material composition in luminescence thermometers based on Fe^{3+} doped AB_2O_4 type nanocrystals (A = Mg, Ca; B = Al, Ga). *Journal of Materials Chemistry C*, Vol. 9, No. 2, 2020, pp. 517–527.

[50] Wang, J. Environmentally friendly Fe^{3+}-activated near-infrared-emitting phosphors for spectroscopic analysis. *Light Sci Appl*, Vol. 11, No. 1, 2022, pp. 178–186.

[51] Zhang, X., D. Chen, X. Chen, C. Zhou, P. Chen, Q. Pang, et al. Broadband near-infrared luminescence from Fe^{3+}-activated $NaScSi_2O_6$ phosphors for luminescence thermometry and night-vision applications. *Dalton Transactions*, Vol. 51, No. 37, 2022, pp. 14243–14249.

[52] Xiang, L., X. Zhou, Y. Wang, L. Li, S. Jiang, G. Xiang, et al. Environmentally-friendly and low-cost Fe^{3+}-doped broadband NIR light-emitting phosphors. *Journal of Luminescence*, Vol. 252, 2022, pp. 119293–119301.

[53] Li, M., Y. Jin, L. Yuan, B. Wang, H. Wu, Y. Hu, et al. Near-infrared long afterglow in Fe^{3+}-activated Mg_2SnO_4 for self-sustainable night vision. *ACS Appl. Mater. Interfaces*, Vol. 15, No. 10, 2016, pp. 13186–13194.

[54] Cheng, K., W. Huang, X. Liu, X. Gong, and C. Deng. Cr^{3+}-free broadband near-infrared phosphors $NaAl_5O_8$: Fe^{3+}. *Journal of Alloys and Compounds*, Vol. 964, 2023, pp. 171240–171248.

[55] Liu, D., G. Li, P. Dang, Q. Zhang, Y. Wei, L. Qiu, et al. Highly efficient Fe^{3+}-doped $A_2BB'O_6$ (A = Sr^{2+}, Ca^{2+}; B, B′ = In^{3+}, Sb^{5+}, Sn^{4+}) broadband near-infrared-emitting phosphors for spectroscopic analysis. *Light: Science & Applications*, Vol. 11, No. 1, 2022, pp. 112–120.

[56] Silva, M. A. F. M. D., S. S. Pedro, and L. P. Sosman. Fe^{3+} concentration dependence of photoacoustic absorption spectroscopy on $ZnGa_2O_4$ ceramic powders. *Spectrochimica Acta Part A Molecular & Biomolecular Spectroscopy*, Vol. 69, No. 2, 2008, pp. 338–342.

[57] Li, M., Y. Jin, L. Yuan, B. Wang, H. Wu, Y. Hu, et al. Near-infrared long afterglow in Fe^{3+}-activated Mg_2SnO_4 for self-sustainable night vision. *ACS Applied Materials & Interfaces*, Vol. 15, No. 10, pp. 13186–13194.

[58] Yang, Y., L. Shen, J. Zhang, S. Zhao, Q. Pang, X. Zhang, et al. Tetracoordinate Fe^{3+} activated Li_2ZnAO_4 (A = Si, Ge) near-infrared luminescent phosphors. *Inorganic Chemistry*, Vol. 62, No. 32, 2023, pp. 12862–12871.